Available online at www.sciencedirect.com
SCIENCE DIRECT®
Journal of Magnetic Resonance 164 (2003) 270–285
JMR Journal of Magnetic Resonance
www.elsevier.com/locate/jmr

Improvement of resolution in solid state NMR spectra with *J*-decoupling: an analysis of lineshape contributions in uniformly ^{13}C-enriched amino acids and proteins

Tatyana I. Igumenova[1] and Ann E. McDermott*

Department of Chemistry, Columbia University, 3000 Broadway MC 3113 New York, NY 10027, USA

Received 31 March 2003; revised 12 June 2003

Abstract

In magic angle spinning (MAS) NMR spectra of highly and uniformly ^{13}C,^{15}N-enriched amino acids and proteins, homo-nuclear coupling interactions contribute significantly to the ^{13}C linewidths, particularly for moderate applied magnetic field strengths and sample spinning frequencies. In this work, we attempted to dissect, analyze, and control the contributions of *J*-coupling and residual homo-nuclear dipolar coupling interactions to the linewidths of uniformly ^{13}C,^{15}N-enriched crystalline alanine; these studies were carried out at 9.4 T using a range of spinning frequencies from 5 to 15 kHz. The anisotropic second-order dipolar shifts and the *J*-splittings are comparable in their contribution to the linewidths, but behave very differently in terms of experimental protocols for line narrowing. In contrast to the *J*-coupling interactions, the second-order dipolar broadening cannot be refocused using selective pulses on the passively coupled spin. We carried out experiments to remove or refocus the ^{13}C *J*-coupling interactions (ω_1 *J*-decoupling) using a selective DANTE pulse in the center of the indirect evolution period. Inversion profiles and bandwidths of selective DANTE pulses acting on transverse magnetization, in the regime of moderate spinning frequencies, were characterized computationally and experimentally. A dramatic improvement in the resolution of the 2D spectrum was achieved when this decoupling protocol was employed.

Keywords: Solid-state NMR; *J*-Decoupling; Second-order dipolar shift; Alanine; Rotational resonance

1. Introduction

Optimal resolution and sensitivity in chemical shift correlation experiments is a prerequisite for the successful spectral assignment and determination of structural constraints in high-resolution solid-state NMR of proteins. A major determinant of the spectral resolution in multidimensional spectra of uniformly ^{13}C,^{15}N-enriched proteins is the ^{13}C linewidth, which, in the absence of structural inhomogeneity of the sample, contains significant contributions from homo- and hetero-nuclear *J*-coupling interactions. Typical ^{1}H-decoupled ^{13}C linewidths in microcrystalline proteins at high applied magnetic field strengths (800 MHz) were reported to be about 100–150 Hz for BPTI [1] and ubiquitin [2]. For comparison, typical one-bond *J*-coupling constants in proteins are 55 Hz for Cα–CO, 35 Hz for Cα–Cβ, 7–11 Hz for N–Cα, and 15 Hz for N–CO atom pairs [3]. Thus, *J*-coupling interactions can contribute as much as 70% to the observed ^{13}C linewidths, at moderate or high field strengths. Homo-nuclear ^{13}C couplings can be greatly reduced by selective ^{13}C enrichment of the alternating carbon sites as described by LeMaster and Kushlan [4] and applied by Hong to solid-state NMR studies of proteins [5,6]. In an alternative approach, the *J*-coupling interactions are refocused during the evolution period in multidimensional NMR experiments (ω_1-decoupling) [7,8].

ω_1 selective decoupling in multidimensional solution NMR experiments has become a routine method for obtaining better resolution in the spectra of biological

* Corresponding author. Fax: +212-932-1289.
E-mail address: aem5@columbia.edu (A.E. McDermott).
[1] Present address: Department of Biochemistry and Biophysics, University of Pennsylvania, Philadelphia, PA 19104-6059, USA.

1090-7807/$ - see front matter © 2003 Elsevier Science (USA). All rights reserved.
doi:10.1016/S1090-7807(03)00239-8

molecules. Various decoupling methods, such as constant time experiments [9–11], amplitude-modulated SEDUCE sequences [12,13], and constant adiabaticity pulses, such as WURST [14,15] have been successfully incorporated into nD NMR pulse sequences. In contrast, there have been only a few examples of ω_1-decoupling in high-resolution solid-state NMR. Straus and co-workers [8,16] reported an application of a selective refocusing method to amino acids and proteins. This method employed a combination of selective and hard π-pulses in the middle of the evolution period in homo- (^{13}C) and hetero-nuclear (^{13}C/^{15}N) chemical shift correlation experiments. For amino acid samples, a reduction in ^{13}C linewidths corresponding to the sum of relevant *J*-coupling constants was reported. This resulted in a significant resolution improvement in 2D ssNMR spectra.

When applied to ssNMR experiments, the combination of hard and selective π pulses has a clear advantage over the out-of-band spin decoupling and constant-time experiments. It is well known that the former introduces non-resonant phase shifts that need to be compensated for [17]. If simple amplitude-modulated selective pulses are used, out-of-band spin decoupling becomes particularly problematic for Cα, since Cβ and C′ have to be decoupled simultaneously. Constant time experiments would be compromised by the fact that the magnitude of *J*-coupling interactions is less than or comparable to the homogeneous and inhomogeneous contributions to the ^{13}C linewidths in amino acids and proteins. For example, the homogeneous ^{13}C linewidth in a microcrystalline formulation of uniformly ^{13}C,^{15}N-enriched ubiquitin was measured to be 30 Hz (T. Igumenova and A. McDermott, unpublished results), while the inhomogeneous broadening due to the second-order dipolar shift was around 53 Hz. Thus, with delays set to 1/2*J* or 9.1 ms for the *J*-coupled Cα–C′ pair, significant signal losses would be expected.

In the present work, we implemented ω_1-decoupling scheme consisting of hard-selective π pulse sandwich (Fig. 1). Good performance of a *J*-decoupling sequence is contingent upon good performance of the selective pulse. Thus our first objective was to optimize the necessary selective pulses, and characterize them in terms of inversion profile, efficiency, and robustness with respect to range of experimental operation. In our experiments, the selective pulse of choice was a Gaussian-modulated DANTE pulse train [18] implemented in the context of a spin pinging sequence [19]. The spin pinging sequence makes use of the centerband DANTE excitation, while the excitation sidebands are placed outside of the spectral region by an appropriate choice of timing between the DANTE pulses. The rationale behind choosing DANTE from a variety of selective pulses available was its simplicity, robustness toward experimental imperfections, and amenability to pulse shaping [20–22].

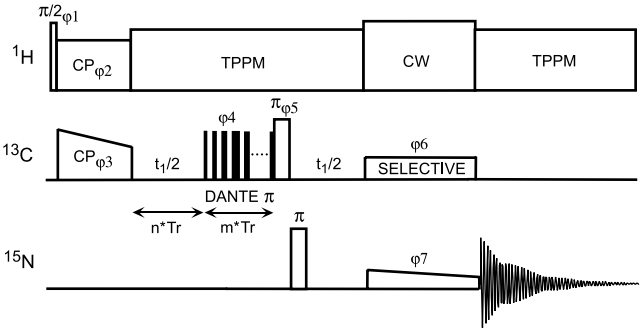

Fig. 1. Double cross-polarization pulse sequence with ω_1-decoupling. Pulse widths in the DANTE pulse train were modulated according to a Gaussian shape function with the truncation amplitude of 5%. The following phase-cycling scheme was used: $\varphi 1 = (x\bar{x})_8$, $\varphi 2 = y$, $\varphi 3 = \bar{y}$, $\varphi 4 = (x)_8(y)_8$, $\varphi 5 = x$, $\varphi 6 = (\bar{y}\bar{y}yy)_4$, $\varphi 7 = (xx\bar{x}\bar{x}yy\bar{y}\bar{y})_2$, and $\varphi_{REC} = (\bar{x}x)_2(\bar{y}y)_2(x\bar{x})_2(y\bar{y})_2$. To ensure that DANTE pulse was always applied on the rotational echo, the dwell time in the indirect dimension was set to twice the rotor period, $2 * Tr$. ^{15}N–^{13}C *J*-decoupling was carried out with a 180° pulse applied on the ^{15}N channel.

Inversion profiles and bandwidths of the DANTE pulses were characterized experimentally and computationally for two spinning frequencies, 5 and 9 kHz. The major issues that arise in this implementation are related to the effect of the substantial chemical shift anisotropy (CSA) of the carbonyl group; these complications are expected for many or all of the selective inversion schemes and thus are generally important phenomena for high-resolution spectroscopy.

Secondly, we analyzed the relative contributions of ^{13}C–^{13}C *J*-coupling and dipolar coupling interactions to ^{13}C linewidths for amino acids and proteins at moderate spinning frequencies and applied field strengths. Three spinning frequency ranges have acceptable properties for spectroscopy of backbone sites in uniformly enriched proteins: the range around 5 kHz for a 400 MHz instrument, or 50 ppm in ^{13}C, which is below the $n = 2$ rotational resonance condition for the ^{13}CO–^{13}Cα pair, the range around 9 kHz, or 90 ppm in ^{13}C, which is between the $n = 2$ and $n = 1$ rotational resonance conditions for the ^{13}CO–^{13}Cα pair, or a range above 25 kHz, or 250 ppm in ^{13}C, which is well above the $n = 1$ rotational resonance condition for the ^{13}CO–^{13}Cα pair. For practical reasons we characterized only the first two cases. The region near 9 kHz is popularly used for protein spectroscopy, since it better minimizes the overlap between carbonyl sidebands and aliphatic centerbands, yet is not technically highly demanding. A clean *J*-coupling doublet is observed only at low (<5 kHz) or ultra-high (>25 kHz) spinning frequencies for the carboxyl site of ^{13}C,^{15}N-enriched alanine. On the other hand, for spinning frequencies (6–10 kHz) often used for protein spectroscopy, the contribution of ^{13}C–^{13}C dipolar couplings to the linewidth is significant. The anisotropic dipolar shifts give rise to a variety of ^{13}C lineshapes, as described previously by Levitt et al. [23]; we analyzed

the specific case for alanine computationally using SIMPSON simulation program [24]. ω_1-decoupling results in almost pure dipolar lineshapes, making it possible to separate contributions of the two interactions to the ^{13}C linewidths. Using sensitivity gain and spectral resolution enhancement as two major criteria, we have characterized the efficiency of *J*-decoupling in the indirect dimension of multidimensional spectroscopy. In this study we show that the best ^{13}C linewidths can be obtained at low spinning frequencies, at the expense of magnetization loss during the selective pulses.

In summary, we have demonstrated that: (i) *J*-decoupling protocol can be efficiently implemented using a DANTE pulse sequence, (ii) chemical shift anisotropy of ^{13}C sites has a profound effect on the performance of selective pulses and *J*-decoupling protocol in general, (iii) in addition to *J*-coupling interactions, there exists another major source of line broadening in uniformly ^{13}C-enriched amino acids and proteins, namely, the ^{13}C homo-nuclear dipolar coupling interactions, which contribution to the linewidth is comparable to that of the *J*-coupling at moderate applied magnetic field strengths. The results reported in this paper have important implications for the choice of experimental conditions for multidimensional ssNMR spectroscopy of proteins at moderate magnetic field strengths.

2. Results and discussion

The results section is divided into three topics relevant to the implementation and success of *J*-decoupling sequences for uniformly ^{13}C,^{15}N-enriched solids. In Section 2.1, we report the characterization of the DANTE inversion pulse; its inversion profile and the effect of the CSA on its performance are discussed. Section 2.2 describes the application of this pulse to ω_1-decoupling in the context of a 2D double cross-polarization experiment; the resolution enhancement produced by *J*-decoupling is evaluated. In Section 2.3, we analyze the free precession and decoupled ^{13}C lineshapes to quantify the relative contributions of homo-nuclear *J*-coupling and dipolar coupling interactions to the ^{13}C linewidth.

2.1. Characterization of the DANTE inversion pulse

The efficiency of *J*-decoupling depends solely on the performance of the selective pulse and its characteristics. To be useful in protein spectroscopy, the inversion pulse acting on a transverse magnetization should have a good inversion profile over a frequency range characteristic for a given spin group in proteins. In addition, the pulse should be kept as short as possible to minimize the magnetization losses due to relaxation. Using these criteria, we characterized the inversion profile of a Gaussian-modulated DANTE pulse train, with the Gaussian amplitude modulation scheme chosen because of its time efficiency. The magnetization losses due to the CSA are assessed from the inversion profiles and magnetization trajectories during the DANTE pulse train.

2.1.1. Inversion profiles

As mentioned in the Introduction, two spinning frequency regimes of practical interest for protein spectroscopy are 50 and 90 ppm. To investigate the effect of the CSA on the performance of the selective pulse, we first consider the case when the selective pulse is applied to the C′ carbon at 50 ppm (5 kHz at 400 MHz field) spinning frequency.

Fig. 2 shows a comparison between a direct (solid line) and inverted (dotted line) ^{13}C′ signals at 5 kHz. The direct signal was obtained with a cross-polarization (CP) sequence, whereas subjecting the CP signal to the DANTE pulse train generated the inverted signal. One can easily see from Fig. 2 that the centerband intensity is preserved in the inverted signal. In contrast, the ($\pm$1) sidebands are positive and their intensity is diminished compared to those of the direct signal. This behavior can be attributed to the effect of the ^{13}C′ CSA, which is non-negligible at a spinning frequency of 5 kHz (see Table 1).

To quantitatively analyze the effect of the CSA on the performance of the DANTE inversion pulse, we follow the treatment of Caravatti et al. [25]. We consider a specific case of the on-resonance centerband inversion, with the starting condition of $\boldsymbol{\rho}(0) = \mathbf{S_X}$. For simplicity, a DANTE pulse train is approximated as a long weak pulse of amplitude $\bar{\omega}_1$ [26]:

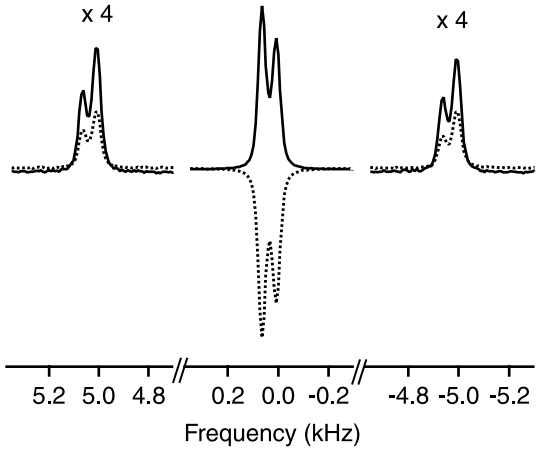

Fig. 2. Comparison of the direct ^{13}C′ signal (—) with the ^{13}C′ signal (· · · ·) subjected to the on-resonance DANTE inversion sequence at a spinning frequency of 5 kHz. The DANTE pulse train consisted of 21 pulses with a total duration of 400 μs. The intensity of the centerband is preserved upon inversion while the sidebands decrease in intensity and become 180° out of phase with the centerband. Under conditions of rotor-synchronized sampling in the 2D experiments, the sidebands are folded onto the centerband, decreasing the intensity of the observed signal.

Table 1
Parameters used in SIMPSON simulations of alanine lineshapes, inversion profiles, and magnetization trajectories

	Cβ	Cα	C′
Chemical shift anisotropy parameters			
δ_{iso} (Hz)[a]	−3093	0	12,643
δ_{aniso} (ppm)	−11.7	−19.7	−71.0
η	0.76	0.44	0.84
$(\alpha_{PC}, \beta_{PC}, \gamma_{PC})$[b]	(−32, 69, 107)	(83, 46, 0)	(−9, 91, −80)
	Cβ–Cα (1.524 Å)	Cα–C′ (1.531 Å)	Cβ–C′ (2.519 Å)
^{13}C dipolar coupling parameters			
b_{IS} (Hz)[c]	−2147	−2117	−475
$(\alpha_{PC}, \beta_{PC}, \gamma_{PC})$	(0, 69, 111)	(0, 0, 0)	(0, 34, 111)
J-Coupling parameters[d]			
	Cβ–Cα	Cα–C′	N–Cα
^1J (Hz)[e]	34.7	55.4	4.0

[a] ^{13}C Larmor frequency is 99.789 MHz.
[b] PC stands for the principal axis to crystal-fixed frame transformation.
[c] b_{IS} is a homo-nuclear dipolar coupling constant defined by the equation $b_{IS} = -(\mu_0\gamma^2\hbar^2/4\pi r_{IS}^3)$, where r_{IS} is the distance between the two nuclei.
[d] *J*-Coupling is assumed to be isotropic.
[e] Measured in solution NMR experiments.

$$\bar{\omega}_1 = \omega_1 \frac{\tau_p}{\tau_d}, \tag{1}$$

where ω_1 is the field strength of DANTE pulses, τ_p is the DANTE pulse duration, and τ_d is the time interval between the pulses. Defining Ω_{PR}^{CSA} as a set of Euler angles relating the principal axis of the CSA tensor to the rotor-fixed frame, a one-spin Hamiltonian can be written as:

$$\mathbf{H} = \omega(\Omega_{PR}^{CSA}; t)\mathbf{S_Z} + \bar{\omega}_1\mathbf{S_Y}, \tag{2}$$

where $\mathbf{S}$ is the spin angular momentum operator for the in-band spin. The Hamiltonian is then transformed to the jolting frame of a particular crystallite having a set of Euler angles (α, β, γ):

$$\tilde{\mathbf{H}} = e^{i\Phi(t)\mathbf{S_Z}}\mathbf{H}e^{-i\Phi(t)\mathbf{S_Z}} = \bar{\omega}_1(\mathbf{S_X}\sin\Phi(t) + \mathbf{S_Y}\cos\Phi(t)) = -\gamma\tilde{\mathbf{B}}_1(t)\mathbf{S}, \tag{3}$$

where $\Phi(t) = \int_0^t \omega(t')\,dt'$. The jolting frame precesses with a time-dependent frequency equal to the chemical shift precession frequency of a given crystallite $\omega(t; \alpha, \beta, \gamma)$. The effective $\tilde{B}_1$ field experienced by the crystallite in the jolting frame is modulated according to the crystallite precession frequency and can be related to the observed NMR signal, $S(t)$, from the following equation:

$$-\gamma\tilde{B}_1(t) = i\bar{\omega}_1\exp^{-i\Phi(t)} = i\bar{\omega}_1 S(t)^*. \tag{4}$$

Expansion of the time-domain signal into a Fourier series produces the following expression for the effective $\tilde{B}_1$ field:

$$-\gamma\tilde{B}_1(t) = i\bar{\omega}_1\sum_{k=-\infty}^{k=\infty} A_k^*\exp^{-ik\omega_r t}, \tag{5}$$

where $A_k = a_k\exp(i\varphi_k)$ is the complex amplitude of the kth sideband. a_k and φ_k are the real amplitude and phase of the kth sideband, respectively. For a perfectly selective on-resonance centerband inversion, only $k = 0$ Fourier component in Eq. (5) is non-zero. The final form of the Hamiltonian in the jolting frame depends on the centerband phase and amplitude as given by Eq. (6):

$$\tilde{\mathbf{H}} = \bar{\omega}_1 a_0(\mathbf{S_X}\sin\varphi_0 + \mathbf{S_Y}\cos\varphi_0). \tag{6}$$

Given the DANTE pulse duration τ_s, the density matrix in the jolting frame can be obtained by the propagation of the initial condition $\boldsymbol{\rho}(0) = \mathbf{S_X}$ under the influence of the Hamiltonian given by Eq. (6)

$$\tilde{\boldsymbol{\rho}}(\tau_s) = a_0[-\sin(\bar{\omega}_1 a_0\tau_s)\mathbf{S_Z} + \cos(\bar{\omega}_1 a_0\tau_s)\cos\varphi_0\mathbf{S_X} - \cos(\bar{\omega}_1 a_0\tau_s)\sin\varphi_0\mathbf{S_Y}]. \tag{7}$$

Performing the transformation from the jolting frame to the lab frame, we obtain the following time dependence of the density matrix:

$$\boldsymbol{\rho}(t) = a_0\{-\sin(\bar{\omega}_1 a_0\tau_s)\mathbf{S_Z} + \cos(\bar{\omega}_1 a_0\tau_s)[\cos\varphi_0 \times (\mathbf{S_X}\cos\Phi(t) + \mathbf{S_Y}\sin\Phi(t)) - \sin\varphi_0 \times (\mathbf{S_Y}\cos\Phi(t) - \mathbf{S_X}\sin\Phi(t))]\}. \tag{8}$$

The signal generated by the time evolution of $\boldsymbol{\rho}(t)$ can be expressed in the compact form as

$$S_{sel}^y(t) = a_0\cos(\bar{\omega}_1 a_0\tau_s)e^{i\Phi(t)}e^{-i\varphi_0}, \tag{9}$$

where superscript y refers to the phase of the selective pulse. The expression for the x DANTE pulse, corresponding to the second step of the spin pinging phase cycle, can be similarly derived

$$S_{sel}^x(t) = a_0 e^{i\Phi(t)}e^{-i\varphi_0}. \tag{10}$$

Eqs. (9) and (10) are similar to those obtained by Caravatti et al. [25] except that we started with the transverse magnetization and treated the case of the

selective inversion pulse. The factor $e^{i\Phi(t)}$ in Eqs. (9) and (10) represents a signal that would be obtained in the case of non-selective inversion. Thus, the effect of CSA is manifested in the presence of the centerband amplitude, a_0, and its phase, φ_0, in the expressions for $S^x_{\rm sel}(t)$ and $S^y_{\rm sel}(t)$. a_0 and φ_0 depend on the orientation of the CSA tensor of a particular crystallite relative to the rotor-fixed frame.

Inspection of Eqs. (9) and (10) allows one to draw the following conclusions. The signal contribution of individual crystallites is scaled by a_0. The $\cos(\bar{\omega}_1 a_0 \tau_s)$ factor in Eq. (9) imposes an orientation dependence on the flip angle. This would inevitably lead to signal loss due to the incomplete inversion of crystallites making a significant contribution to the sidebands. The phase factor $e^{-i\varphi_0}$ creates an orientation dependent phase distribution of the crystallite magnetizations at the beginning of the sampling period. This means that the amplitude and phase of the sideband family will be different from that observed in non-selective experiments.

To examine more closely what happens with the sideband family after the selective inversion pulse, we expanded the non-selective signal, $e^{i\Phi(t)}$, within the expression for the signal resulting from the selective pulse, into the following Fourier series:

$$\begin{aligned} S^x_{\rm sel}(t) &= a_0 \sum_{k=-\infty}^{k=\infty} a_k e^{i(\varphi_k-\varphi_0)} e^{ik\omega_r t} \\ &= a_0^2 + \sum_{\substack{k=-\infty \\ k\neq 0}}^{k=\infty} a_k a_0 e^{i(\varphi_k-\varphi_0)} e^{ik\omega_r t} \\ &= a_0^2 + \sum_{\substack{k=-\infty \\ k\neq 0}}^{k=\infty} A_k A_0^* e^{ik\omega_r t}. \end{aligned} \tag{11}$$

It is clear from Eq. (11) that each crystallite makes a positive absorptive contribution to the centerband, which is scaled by the $\cos(\bar{\omega}_1 a_0 \tau_s)$ factor in the case of the orthogonal pulse (Eq. (9)). There is no cancellation effect due to the dispersive centerband components as in the case of a non-selective signal. This can lead to a selective enhancement of the irradiated sideband in the case of selective excitation [25]. The sideband amplitudes can be determined from Eq. (11) using the following symmetry relationship [27]:

$$A_k(\Omega_{PR}^{CSA}) = A_k^*(\Omega_{PR}^{\prime CSA}) \tag{12}$$

where $\Omega_{\rm PR}^{\rm CSA} = (\alpha, \beta, \gamma)$ and $\Omega_{\rm PR}^{\prime\rm CSA} = (-\alpha, \beta, -\gamma)$. When doing the powder averaging of Eq. (11), for a given crystallite orientation it is always possible to find another one that cancels out the dispersive components. Thus, the entire sideband family of the signal produced by the DANTE inversion pulse is absorptive. This is indeed what we observe in the experiments (see Fig. 2, dotted trace). Numerical simulations show that in the absence of the spin pinging phase cycling, there is a slight phase distortion of the sidebands, which is due to the large bandwidth of the inversion pulses that we used. The assumption of perfect selectivity used in the derivation of Eq. (6) is no longer valid in the case of large bandwidth pulses. However, the spin pinging phase cycle eliminates the phase distortions resulting in absorptive sidebands.

The performance of the selective pulse applied to the Cα carbon at 5 kHz spinning frequency is similar to that of the C′ (data not shown). It is worth noting that when large bandwidth pulses are used in the low spinning frequency regime, there is a possibility of accidentally establishing a HORROR matching condition [28] between Cα and Cβ, i.e., $(0.5/\tau_s) \times (1+\sqrt{1+(2\tau_s \Delta)^2}) = \omega_r$, where Δ is the difference between the isotropic chemical shifts of Cα and Cβ. This would result in the deterioration of the Cα signal.

Experimental and simulated inversion profiles for Cα/Cβ and C′ carbons at a spinning frequency of 9 kHz are presented in Fig. 3. The agreement between the experiments and simulations is excellent, with all profiles having a Gaussian shape. The parameters of selective pulses were chosen based on the chemical shift ranges of Cα and CO found in proteins. For example, in ubiquitin the chemical shift ranges are 12.5 and 11 ppm for Cα and CO, respectively. Fig. 3a shows the experimental and simulated inversion profiles of a 666.7 μs DANTE pulse for Cα (circles) and Cβ (diamonds). For Cα, it is important to find a compromise between the bandwidth required for the inversion over a certain chemical shift range and the selectivity necessary for efficient decou-

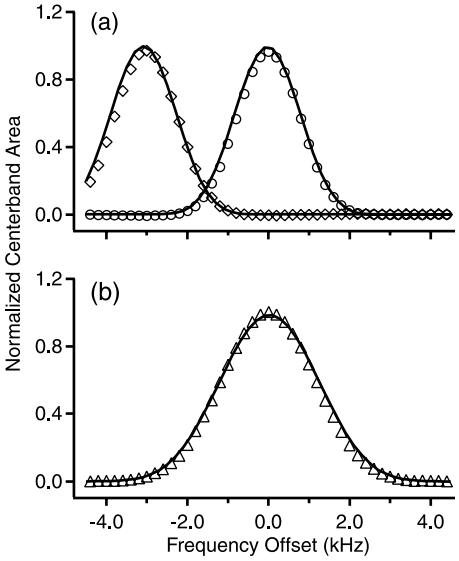

Fig. 3. Inversion profiles of (a) ^{13}Cα/Cβ and (b) ^{13}C′ centerbands at a spinning frequency of 9 kHz. Experimental Cα (○) and Cβ (◇) data were collected with a 666.7 μs DANTE pulse train, while for the C′ inversion profile (△) a 444.4 μs DANTE pulse was used. Solid lines show simulated profiles.

pling from Cβ. In alanine, the difference between Cα and Cβ chemical shifts is 31 ppm. The 666.7 μs DANTE pulse applied on the Cα resonance, gives a negligible Cβ excitation and 72% Cα inversion over the bandwidth of ±600 Hz. For the CO spins in proteins, the bandwidth can be made rather substantial without affecting other spins. Fig. 3b shows the inversion profile of a 444.4 μs DANTE pulse applied on the C′ resonance of alanine. This pulse gives 88% inversion over the bandwidth of ±600 Hz.

2.1.2. Magnetization trajectories

To estimate the extent of signal retention obtained in *J*-decoupling experiments, we simulated the magnetization trajectories for C′ and Cα, shown in Fig. 4. The red and black traces correspond to spinning frequencies of 5 and 9 kHz, respectively. Only trajectories for the orthogonal pulse are shown. The experimental signal retention was calculated as a ratio of cross-peak volumes obtained in the decoupled and free precession 2D experiments.

First, we consider the case of C′ at a spinning frequency of 5 kHz (Fig. 4a, red trace). At the end of the inversion pulse, the *Ix* component makes 39% of the initial signal intensity. This signal loss can be attributed to two factors: (i) orientation dependence of the flip angle and signal scaling by a_0; and (ii) initial phase distribution of crystallite magnetizations (see Eq. (9)). The latter causes the crystallite magnetizations to interfere destructively in the course of the free precession following the inversion pulse. Numerical simulations show that, when the selective pulse of the same phase as the initial magnetization is applied (Eq. (10)), only 61% of the C′ signal is retained. The average value of the signal retention obtained in numerical simulations is 50%, which agrees well with the 55% obtained in experiments.

The magnetization trajectory of the C′ spin at 9 kHz is also affected by the CSA (Fig. 4a, black trace). The simulated signal retention is 77% compared to the experimental value of 80%. Note that, for both spinning frequency regimes, there is no appreciable *Iy* component build-up during the DANTE pulse train.

The situation with Cα is different since both spinning frequencies far exceed the Cα CSA. At 5 kHz (Fig. 4b, red trace), we notice that there is a non-negligible *Iy* component appearing during the DANTE pulse train. This is due to a partial HORROR recoupling between Cα and Cβ (see above). Cα magnetization at 9 kHz (Fig. 4b, black trace) follows an almost perfect inversion trajectory, resulting in 94% magnetization retention.

Although the expressions derived above are for an inversion profile only, we have carried out numerical simulations to study the performance of these pulses in the context of the 2D experiment, i.e., including the

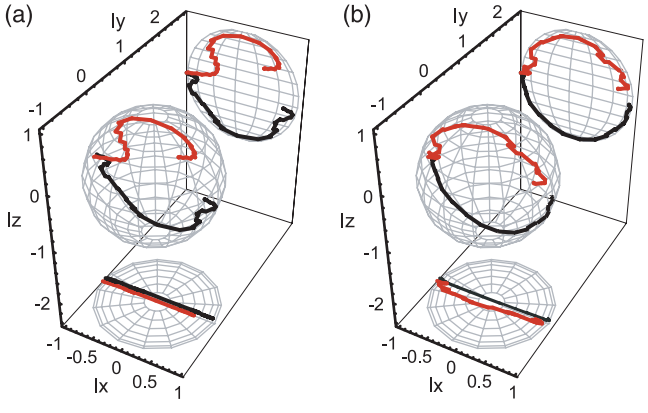

Fig. 4. Simulated magnetization trajectories of $^{13}C'$ (a) and $^{13}C\alpha$ (b) during the DANTE pulse train. Red and black traces correspond to the spinning frequencies of 5 and 9 kHz, respectively. At 5 kHz, the duration of the DANTE pulse was 1.2 ms for Cα and 400 μs for C′. At 9 kHz, the duration of DANTE pulse was 666.7 μs for Cα and 444.4 μs for C′. The magnetization components *Ix*, *Iy*, and *Iz* were sampled twice per each DANTE "pulse-delay" unit.

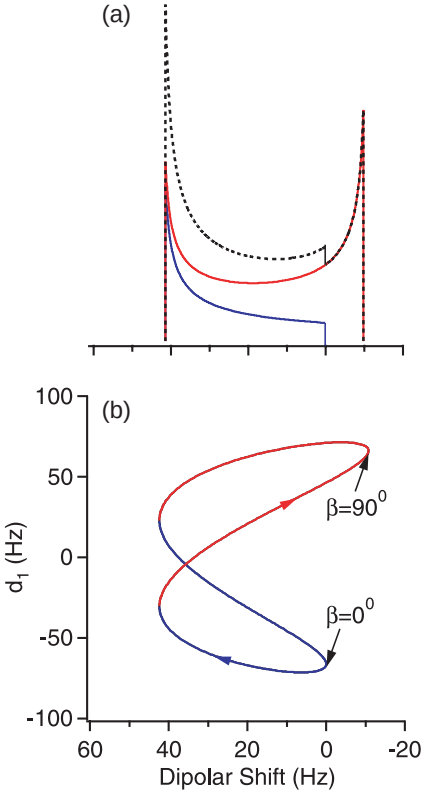

Fig. 10. Orientation dependence of (a) the second-order dipolar shift and (b) ^{15}N–^{13}C polarization transfer for the $^{13}C'$ of alanine. Blue traces correspond to angle β in the range of 0–43.4° and 136.6–180°, and red traces correspond to angle β in the range of 43.4–136.6°. In Graph a, powder patterns were simulated using Eq. (27), with the dotted line showing the sum of individual powder patterns. Graph b is a parametric plot of the ZQ dipolar-coupling element (Eq. (28)) versus the second-order dipolar shift (Eq. (26)). The crystallites with higher statistical weight have a smaller effective dipolar-coupling element, which explains why the experimental decoupled $^{13}C'$ lineshape appears inverted compared to the simulations in Fig. 7.

chemical shielding terms and appropriate delays. The imperfections of the inversion pulse, while having a dramatic effect upon signal retention, have very subtle or negligible effects on the quality of decoupling and resulting lineshapes. This is another advantage of utilizing an in-band selective inversion sequence.

Numerical simulations of soft square and Gaussian-shaped pulses acting on the transverse magnetization showed inversion profiles and sideband patterns identical to those of the square and Gaussian-shaped DANTE pulse trains. This leads to a general observation that when selective pulses are used in the context of *J*-decoupling, one should expect some signal loss in the cases when the CSA is less than or comparable to the spinning frequency.

2.2. Experimental ^{13}C lineshapes in uniformly $^{13}C,^{15}N$-enriched alanine. J-decoupling in double cross-polarization experiments

2.2.1. 1D ^{13}C CP MAS spectra of alanine

To assess the relative contribution of ^{13}C–^{13}C *J*-coupling and dipolar coupling interactions to ^{13}C linewidth, we recorded a series of 1D ^{13}C CP MAS spectra of uniformly ^{13}C,^{15}N-enriched microcrystalline alanine at different spinning frequencies. Expanded spectral regions showing the carboxyl resonance of alanine are presented in Fig. 5. In the same figure, the experimental spectra are compared with the results of three-spin SIMPSON simulations carried out with the parameters listed in Table 1. Both the experimental and simulated spectra are plotted on the same chemical shift scale.

The most interesting feature of the data is a pronounced dependence of the lineshape and chemical shift on the spinning frequency. The chemical shift difference between C′ and Cα atoms in alanine, $\omega_{\Delta}^{\mathrm{iso}}$, is 12.6 kHz with the spinning frequencies of 12.6 and 6.3 kHz corresponding to $n = 1$ and $n = 2$ rotational resonance conditions. Rotational resonance conditions occur when the difference in isotropic chemical shifts of the two dipolar-coupled nuclei matches a multiple of the spinning frequency [29]: $\omega_{\Delta}^{\mathrm{iso}} = n\omega_r$, where n is a small integer. As evident from Fig. 5, significant changes in ^{13}C lineshape occur not only in the immediate vicinity of the rotational resonance conditions, but also over the entire range of spinning frequencies from 6 to 13 kHz. At spinning frequencies near or below 5 kHz, we observe a doublet suggesting that the C′–Cα *J*-coupling interaction makes a major contribution to the overall linewidth. Starting from 6 kHz, the carboxyl resonances acquire triplet-like features that then persist for the entire range of spinning frequencies between the $n = 1$ and $n = 2$ rotational resonance conditions. We conclude that $n = 1$ and $n = 2$ rotational resonance conditions are rather broad with the non-secular "flip-flop" part of the homo-nuclear dipolar Hamiltonian contributing appreciably to the ^{13}C lineshape and linewidth. This effect is most evident at moderate applied magnetic field strengths. At high fields, the "flip-flop" term is truncated by the large chemical shift difference term.

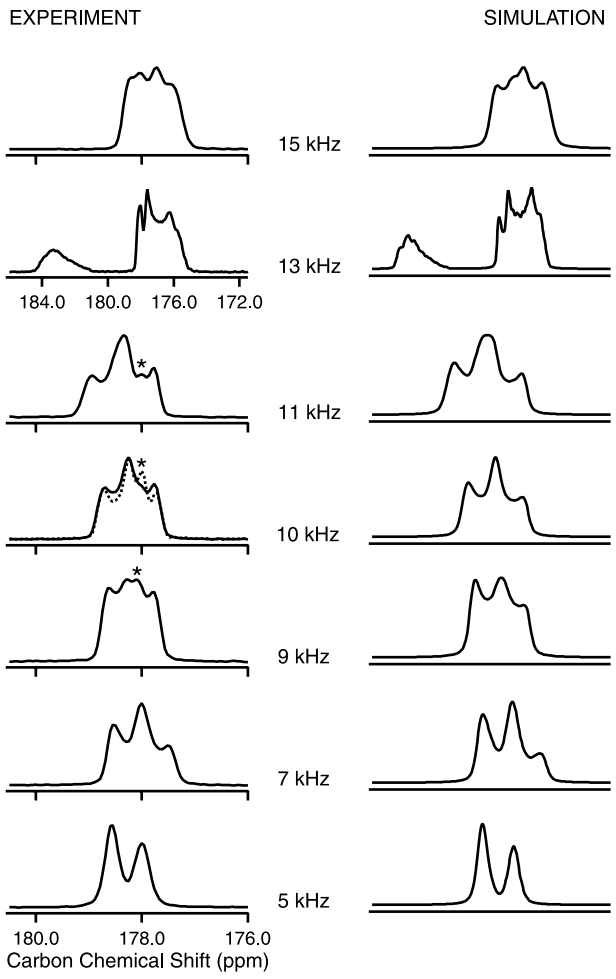

Fig. 5. Experimental and simulated $^{13}C'$ lineshapes in uniformly ^{13}C,^{15}N-enriched alanine as a function of spinning frequency. The spectrum of 14% uniformly ^{13}C,^{15}N-enriched/86% natural abundance alanine at a spinning frequency of 10 kHz is shown with a dotted line. Peaks corresponding to natural abundance alanine are marked with an asterisk. Ramped cross-polarization was carried out on the (+1) matching sideband condition for ^{13}C with $\omega_1(^1H) = 50$ kHz. To emphasize the lineshape details, experimental data sets were zero-filled four times and apodized using the Lorentzian-to-Gaussian windowing function. The same apodization function was applied to the simulated data.

Fig. 6 shows a plot of the simulated free precession (circles) and *J*-decoupled (diamonds) C′ full width at half height (FWHH) as a function of spinning frequency. The C′ chemical shift dispersion due the second-order dipolar shift, given by Eq. (26), is shown with a dotted line. A comparison of the free precession and *J*-decoupled C′ linewidths clearly indicates that the two spinning frequency regimes that will benefit from *J*-decoupling are around 5 and 9 kHz. The analytical prediction of the C′ chemical shift dispersion follows the

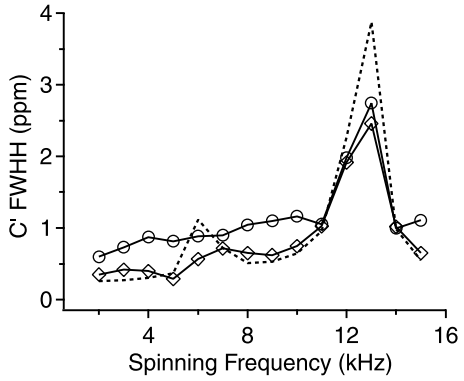

Fig. 6. Full width at half height (FWHH) of the simulated free precession (○) and *J*-decoupled (◇) $^{13}C'$ resonances as a function of spinning frequency. C′ chemical shift dispersion due to the second-order dipolar shift, given by Eq. (26), is shown with a dotted line. Spinning frequency regimes that will benefit from *J*-decoupling are around 5 and 9 kHz.

same trend as the *J*-decoupled linewidths, providing an estimate of the contribution of the homo-nuclear ^{13}C dipolar couplings to the observed ^{13}C linewidths.

Qualitatively, agreement between the experimental and simulated lineshapes is good (see Fig. 5) with only a small difference between the two. This discrepancy may be attributed to the following factors. First, the experimental spectra at 9, 10, and 11 kHz clearly show the presence of an extra peak marked by an asterisk in Fig. 5. A comparison between the $^{13}C'$ signal of the uniformly enriched alanine (solid line) and that of the co-crystallized mixture of 14% uniformly enriched/86% natural abundance alanine (dotted line) at 10 kHz shows that this peak is likely to originate from the single-labeled and natural abundance impurities. The peak has a pronounced effect on the lineshape and appears at the chemical shift different from those of the "triplet" components. Secondly, in SIMPSON simulations, T_2 relaxation was introduced as an exponential apodization function with a line-broadening parameter of 19 Hz corresponding to the FWHH of the carboxyl peak in natural abundance alanine. The contribution of inter-molecular ^{13}C dipolar interactions was not taken into account.

In addition to its effect on the lineshape and linewidth, the non-resonant components of the "flip-flop" dipolar term interact with Zeeman energy levels causing a change in the chemical shift as described by several authors [23,30]. The spinning frequency dependent dipolar shifts of $^{13}C'$ peaks are evident in Fig. 5 for both the experimental and simulated spectra that are in excellent agreement with each other.

The spinning frequency dependence of Cα lineshapes shows the same trend as that of C′ (data not shown). However, the Cα lineshapes are more complex due to the *J*-coupling and dipolar coupling interactions with Cβ. The Cβ peak is a clean *J*-coupling doublet everywhere except in the vicinity of 3.1 kHz, which corresponds to the $n = 1$ rotational resonance condition between Cα and Cβ.

2.2.2. Homo-nuclear ^{13}C *J*-decoupling

From the spinning frequency dependence of the carboxyl lineshapes it becomes clear that the narrowest linewidths can be obtained at a spinning frequency of 5 kHz and below. In contrast, at 9 kHz, which is our spinning frequency of choice for protein spectroscopy, the carboxyl lines are rather broad and have a characteristic triplet lineshape. Given the similarity of tensorial interactions in amino acids and proteins, lower spinning frequencies could probably be exploited to achieve higher resolution in multidimensional solid-state NMR of proteins.

To investigate the lineshapes further and establish the extent of line-narrowing that could be obtained, we carried out 2D ^{13}C–^{15}N chemical shift correlation experiments with homo-nuclear ^{13}C *J*-decoupling in the indirect dimension. The pulse sequence used in the experiments is shown in Fig. 1 and is based on the work of Straus et al. [8]. *J*-decoupling is achieved by a pair of π pulses, soft and hard, placed in the middle of the t_1 evolution period. The pulses produce a net 2π rotation of the in-band and a π rotation of the out-of-band spin magnetizations, refocusing the *J*-coupling interaction during t_1.

Free precession (FP) and decoupled (DEC) lineshapes of the carboxyl resonance of alanine at two spinning frequencies, 5 and 9 kHz, are shown in Fig. 7. The experimental data represent the cross-sections taken through the ^{13}C–^{15}N cross-peaks. In the same figure, the experimental data are compared with simulations. The simulations of the decoupled experiments were carried out setting the relevant *J*-coupling constants to zero and incorporating the π-pulse sandwich element to account for the signal losses due to the chemical shift anisotropy. To estimate the apparent sensitivity gain, the intensities of decoupled resonances were normalized to those of the free precession peaks. The linewidths, determined as the full widths at half-height, are presented in Table 2, and demonstrate an excellent agreement between the experiments and simulations. As evident from Table 2 for both spinning frequencies, the reduction in $^{13}C'$ linewidth is approximately equal to the C′–Cα *J*-coupling constant.

At a spinning frequency of 9 kHz, the decoupled lineshape has a form of a doublet with asymmetric intensities of its components. The origin of this lineshape lies in the orientation-dependent second-order energy shifts caused by the non-secular terms of the homo-nuclear dipolar coupling Hamiltonian. Since the ^{13}C lineshapes are detected in the indirect dimension, the orientation dependence of the transfer efficiency imposed by a given mixing sequence makes a contribution to the lineshape as well, explaining the difference

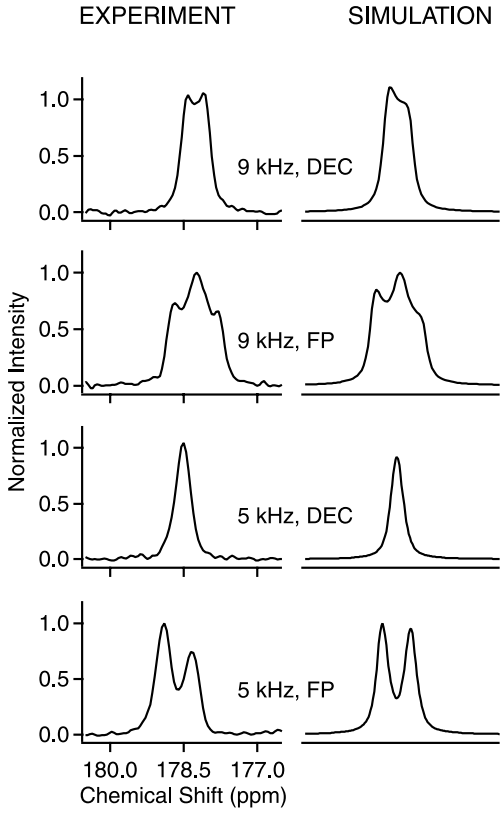

Fig. 7. *J*-decoupled (DEC) and free-precession (FP) $^{13}C'$ spectra at two spinning frequencies, 5 and 9 kHz. Experimental spectra are the cross-sections through the ^{15}N resonance of the 2D ^{15}N–$^{13}C'$ double cross-polarization spectra. The ZQ ^{13}C–^{15}N double cross-polarization was carried out using the following field strengths: $\omega_1(^{13}C) = 22.5$ kHz and $\omega_1(^{15}N) = 13.5$ at 9 kHz; $\omega_1(^{13}C) = 17.5$ kHz and $\omega_1(^{15}N) = 12.5$ at 5 kHz. In *J*-decoupled experiments, the DANTE pulse train consisted of 21 Gaussian-modulated pulses, with a total duration of four rotor periods at 9 kHz and two rotor periods at 5 kHz. Simulations of *J*-decoupled spectra were carried out in a pseudo 1D mode, setting the relevant *J*-coupling constants to zero and including the soft and hard 180° pulses. The latter was done to account for the signal loss during the DANTE pulse train. Pseudo 1D simulations with relevant *J*-coupling constants turned off and 2D simulations with ω_1-decoupling were found to produce identical results. Simulated spectra were processed with an exponential linebroadening value of 19 Hz.

between the experiments and simulations. The aspects of the orientation dependence of the second-order dipolar shift and transfer efficiency will be treated quantitatively in Section 2.3 of this paper. The difference between the FWHH of the natural abundance and *J*-decoupled $^{13}C'$ peaks is 42 Hz, which puts an upper limit on the contribution of homo-nuclear dipolar coupling interactions to the ^{13}C linewidths. Further splitting of the dipolar pattern by the *J*-coupling interaction with Cα produces the characteristic triplet-like lineshapes that we observe in the 1D ^{13}C spectra.

At a spinning frequency of 5 kHz, the contribution of homo-nuclear dipolar coupling interactions to the $^{13}C'$ linewidth is negligible, with the *J*-coupling interaction dominating the linewidth. The *J*-coupling doublet is asymmetric due to the coherent cross-correlation of the CSA and dipolar coupling tensors [31]. It is evident from Fig. 7 that lines as narrow as 36 Hz could be obtained if the *J*-coupling interactions are removed. However, there is little sensitivity gain in the decoupled spectra as indicated by similar intensities of the free precession and decoupled C′ peaks.

Decoupled and free precession lineshapes for the Cα carbon are shown in Fig. 8 and the corresponding linewidths are given in Table 2. For the both spinning frequencies, 5 and 9 kHz, *J*-decoupling from C′ and Cβ reduces the Cα linewidths by 50–60 Hz. In contrast to the C′ resonance, no dramatic difference between the decoupled linewidths at 5 and 9 kHz is observed for the Cα peak. This is due to the fact that the contribution of the Cα–Cβ dipolar coupling to the Cα linewidth is non-negligible at 5 kHz, which is close to the $n = 1$ rotational resonance condition between Cα and Cβ. Overall, the sensitivity gain obtained in the *J*-decoupled experiments is larger for Cα than that for C′.

In summary, Table 2 indicates very good agreement for C′ and Cα linewidths obtained in experiments and simulations. Since the simulations were performed with the *J*-coupling interactions completely turned off, this agreement proves that the experimental implementation of the *J*-decoupling is very efficient. The extent of the resolution enhancement can be readily evaluated from the 2D slices shown in Figs. 7 and 8, while the observed sensitivity gain is in fact a combination of the lineshape effect and the overall signal retention in the indirect dimension. The C′ peak at 9 kHz can be considered as an example of the lineshape effect. Its free-precession lineshape is triplet-like, with dipolar and *J*-coupling contributing almost equally to the linewidth. The removal of *J*-coupling thus produces only a modest signal enhancement.

Table 2
Free precession and *J*-decoupled linewidths (FWHH) of C′ and Cα carbons of alanine

	C′		Cα	
Spinning frequency (kHz):	5	9	5	9
Free precession linewidth (Hz)	90 (86)[a]	112 (112)	120 (120)	113 (118)
Decoupled linewidth (Hz)	36 (30)	61 (64)	65 (65)	60 (63)
Difference (Hz)	54 (56)	51 (48)	60 (55)	53 (55)

[a] Linewidths obtained in simulations are given in parenthesis.

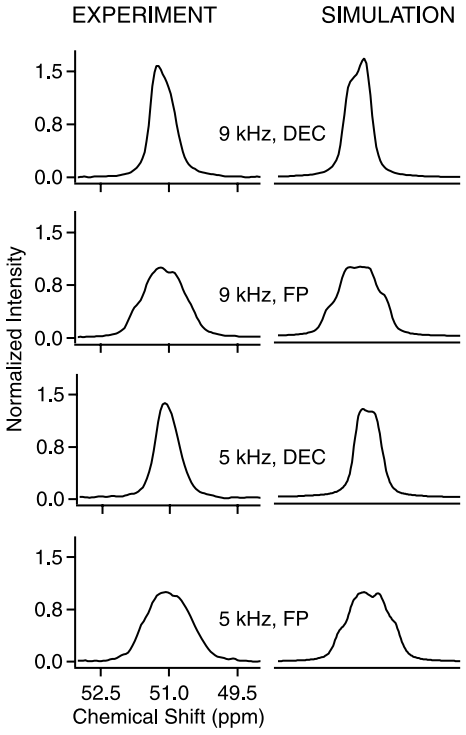

Fig. 8. *J*-decoupled (DEC) and free-precession (FP) $^{13}C\alpha$ spectra at two spinning frequencies, 5 and 9 kHz. Experimental spectra are the cross-sections through the ^{15}N resonance of the 2D ^{15}N–$^{13}C\alpha$ double cross-polarization spectra. The ZQ ^{13}C–^{15}N double cross-polarization was carried out using the following field strengths: $\omega_1(^{13}C) = 22.5$ kHz and $\omega_1(^{15}N) = 13.5$ at 9 kHz; $\omega_1(^{13}C) = 17.5$ kHz and $\omega_1(^{15}N) = 12.5$ at 5 kHz. In *J*-decoupled experiments, the DANTE pulse train consisted of 21 Gaussian-modulated pulses, with a total duration of six rotor periods. Simulations of *J*-decoupled spectra were carried out in the 1D mode, setting the relevant *J*-coupling constants to zero and including the soft and hard 180° pulses. The latter was done to account for signal loss during the DANTE pulse train. Pseudo-1D simulations with relevant *J*-coupling constants turned off and 2D simulations with ω_1-decoupling were found to produce identical results. Simulated spectra were processed with an exponential linebroadening value of 19 Hz.

2.3. Orientation dependence of the second-order dipolar shift

To analyze the free precession and *J*-decoupled ^{13}C lineshapes quantitatively, we made use of the functional dependence of the second-order dipolar shift on the relative orientation of the dipolar coupling tensor and the rotor axis. A full derivation of this functional dependence is given in [23,30]. Here, we present a short summary of this derivation to facilitate the discussion of the experimentally observed second-order dipolar shift.

We consider a homo-nuclear system of two spins 1/2, *S* and *I* that are assumed to have different chemical shifts. For simplicity, we disregard the *J*-coupling interaction between *S* and *I*. The high-field truncated Hamiltonian of this system includes chemical shift terms for two spins and the homo-nuclear dipolar coupling term, $\mathbf{H}_{IS}$, as follows:

$$\mathbf{H}(t) = \omega_I(t)\mathbf{I_Z} + \omega_S(t)\mathbf{S_Z} + \mathbf{H}_{IS}(t), \tag{13}$$

where $\omega_I(t)$ and $\omega_S(t)$ are the chemical shift precession frequencies of spins *S* and *I*. The time dependence is imposed on the Hamiltonian by magic angle spinning. The homo-nuclear dipolar coupling term $\mathbf{H}_{IS}$ can be expressed as a sum of the secular and non-secular contributions, $\mathbf{H}^{\mathrm{A}}_{IS}$ and $\mathbf{H}^{\mathrm{B}}_{IS}$:

$$\begin{aligned}\mathbf{H}_{IS}(t) &= \mathbf{H}^{\mathrm{A}}_{IS}(t) + \mathbf{H}^{\mathrm{B}}_{IS}(t)\\ &= \omega_D(t)2\mathbf{I_Z}\mathbf{S_Z} - \omega_D(t)\frac{1}{2}(\mathbf{I}_+\mathbf{S}_- + \mathbf{I}_-\mathbf{S}_+).\end{aligned} \tag{14}$$

The secular part $\mathbf{H}^{\mathrm{A}}_{IS}$ gives rise to the first-order corrections to the Zeeman energy levels and is averaged to zero over a rotor period. The non-secular part $\mathbf{H}^{\mathrm{B}}_{IS}$, sometimes referred to as the "flip-flop" part of the $\mathbf{H}_{IS}$, perturbs the Zeeman eigenstates and is responsible for the second-order energy shifts. To derive the time and orientation dependence of $\omega_D(t)$, we introduce three coordinate frames: the laboratory frame, *L*; the principal axis system of the dipolar coupling tensor, *P*; and the rotor-fixed frame, *R*. Transformations between these coordinate systems can be carried out using two sets of Euler angles, $\Omega_{\mathrm{PR}}(0,\beta,\gamma)$ and $\Omega_{\mathrm{RL}}(\omega_r t,\theta,0)$, as follows:

$$P \xrightarrow{\Omega_{\mathrm{PR}}(0,\beta,\gamma)} R \xrightarrow{\Omega_{\mathrm{RL}}(\omega_r t,\theta,0)} L. \tag{15}$$

Rotation of the dipolar coupling tensor from the principal axis system to the laboratory frame via the rotor-fixed frame is accomplished using Wigner rotation matrices:

$$\begin{aligned}\omega_D(t;\Omega_{\mathrm{PR}}) &= b_{IS}\sum_{m=-2}^{m=2} D^{(2)}_{-m,0}(\omega_r t,\theta,0)D^{(2)}_{0,-m}(0,\beta,\gamma)\\ &= b_{IS}\sum_{m=-2}^{m=2} \mathrm{e}^{\mathrm{i}m\omega_r t} d^{(2)}_{-m,0}(\theta)D^{(2)}_{0,-m}(0,\beta,\gamma)\\ &= \sum_{m=-2}^{m=2} \omega_D^{(m)}(\Omega_{\mathrm{PR}})\mathrm{e}^{\mathrm{i}m\omega_r t},\end{aligned} \tag{16}$$

where the dipolar coupling constant b_{IS} is given by Eq. (17)

$$b_{IS} = -\left(\frac{\mu_0}{4\pi}\right)\frac{\gamma^2\hbar^2}{r^3_{IS}}. \tag{17}$$

At the "magic angle," $\theta = 54.73°$, the following equations for the Fourier coefficients $\omega_D^{(m)}$ are obtained:

$$\omega_D^{(1)} = -b_{IS}\frac{\sin 2\beta}{\sqrt{8}}\mathrm{e}^{\mathrm{i}\gamma} = \omega_D^{(-1)*}, \tag{18}$$

$$\omega_D^{(2)} = b_{IS}\frac{\sin^2\beta}{4}\mathrm{e}^{2\mathrm{i}\gamma} = \omega_D^{(-2)*}. \tag{19}$$

To treat the case of rotational resonance for the IS spin pair, Gan and Grant [30] first factored out the evolution of $|\alpha\beta\rangle$ and $|\beta\alpha\rangle$ states from the Hamiltonian of Eq. (13). Eq. (20) provides an expression for the corresponding sub-matrix calculated in the product basis:

$$\mathbf{H_K} = \frac{1}{2}\begin{bmatrix} \omega_I(t) - \omega_S(t) & \omega_D(t) \\ \omega_D(t) & -\omega_I(t) + \omega_S(t) \end{bmatrix}. \tag{20}$$

The matrix of Eq. (20) describes nutation of a pseudo-spin 1/2, denoted below as K, around magnetic field $\omega_D(t)$. The four-level system that we started with is thus effectively reduced to two levels. Re-writing Eq. (20) in spin-operator terms results in the following expression for the pseudo-spin Hamiltonian:

$$\mathbf{H_K} = \Delta\omega(t)\mathbf{K_Z} + \omega_D(t)\mathbf{K_X}, \tag{21}$$

where $\Delta\omega(t) = \omega_I(t) - \omega_S(t)$ is the difference between the precession frequencies of spins S and I. First-order average Hamiltonian theory is then applied to render $\mathbf{H_K}$ time-independent. To make the average Hamiltonian series converge, $\mathbf{H_K}$ is transformed to the rotating frame of pseudo-spin K using propagator $\mathbf{U_R} = \exp(\mathrm{i}n\omega_r t\mathbf{K_Z})$:

$$\tilde{\mathbf{H}}_\mathbf{K} = (\Delta\omega(t) - n\omega_r)\mathbf{K_Z} + \omega_D(t)(\mathbf{K_X}\cos(n\omega_r t) - \mathbf{K_Y}\sin(n\omega_r t)). \tag{22}$$

Average $\tilde{\mathbf{H}}_\mathbf{K}$ (denoted $\tilde{\mathbf{H}}^{\mathbf{av}}_\mathbf{K}$) calculated to the first order can be expressed as a product of pseudo-spin operator $\mathbf{K}$ and effective magnetic field $\mathbf{B_{eff}}$ experienced by the pseudo-spin:

$$\tilde{\mathbf{H}}^{\mathbf{av}}_\mathbf{K} = \mathbf{B_{eff}}\mathbf{K}. \tag{23}$$

If the chemical shift anisotropy is neglected, the x and y components of $\mathbf{B_{eff}}$ vanish, leaving only the z term in the final expression for $\tilde{\mathbf{H}}^{\mathbf{av}}_\mathbf{K}$ as follows:

$$\tilde{\mathbf{H}}^{\mathbf{av}}_\mathbf{K} = \left((\omega_\Delta^{\mathrm{iso}} - n\omega_r) + \frac{1}{2\omega_r}\sum_{\substack{k=-2 \\ k\neq 0}}^{k=2} \frac{n\left|\omega_D^{(k)}\right|^2}{n^2 - k^2}\right)\mathbf{K_Z}, \tag{24}$$

where $\omega_\Delta^{\mathrm{iso}}$ is the difference between the isotropic chemical shifts of S and I. Taking the diagonal matrix elements of this Hamiltonian with the $|\alpha\rangle$ and $|\beta\rangle$ pseudo-spin states produces the following corrections to the pseudo-spin energy levels:

$$\Delta^{(2)} = \pm\frac{1}{4}\sum_{\substack{k=-2 \\ k\neq 0}}^{k=2} \frac{\left|\omega_D^{(k)}\right|^2}{\omega_\Delta^{\mathrm{iso}} - k\omega_r}. \tag{25}$$

Referencing Eq. (25) back to the four-level system of spins S and I, we notice that the shift will be positive for the $|\alpha\beta\rangle$ state and negative for the $|\beta\alpha\rangle$ state. The energy corrections given by Eq. (25) are referred to as the second-order shifts, since the calculation of the Hamiltonian to first order in the average Hamiltonian theory is equivalent to having a second-order term in the Hamiltonian perturbation expansion. Using the latter in combination with Floquet theory, Levitt and co-workers [23] obtained an identical expression for the second-order shift. Meier and Earl [32] presented a particular case of the second-order dipolar shift under conditions of slow spinning. Their result is readily obtainable from Eq. (25) by assuming $k\omega_r \ll \omega_\Delta^{\mathrm{iso}}$. Combining Eqs. (18), (19), and (25), one arrives at an explicit expression for the functional dependence of the second-order dipolar shift on the angle (β) between the inter-nuclear vector and rotor axis:

$$\Delta^{(2)} = \pm\frac{\omega_\Delta^{\mathrm{iso}} b_{IS}^2}{4}\left(\frac{\sin^2\beta\cos^2\beta}{(\omega_\Delta^{\mathrm{iso}})^2 - \omega_r^2} + \frac{1/8\sin^4\beta}{(\omega_\Delta^{\mathrm{iso}})^2 - 4\omega_r^2}\right). \tag{26}$$

It is clear from Eq. (26) that the second-order dipolar shift produces orientation-dependent broadening of S and I resonances. Thus, the S and I resonances are inhomogeneously broadened in that they consist of separate lines, each of which can be manipulated individually. The shift makes a positive contribution to the transition frequency of spin I, and a negative contribution to that of spin S. This behavior manifests itself spectrally in the fact that (i) the lineshapes of S and I are mirror images of one another, and (ii) the resonance of spin I shifts downfield, whereas the resonance of spin S shifts upfield.

The C′–Cα spin pair of alanine is a specific example of the aforementioned behavior. To determine the extent of inhomogeneous broadening caused by the second-order dipolar shift, we carried out numerical simulations of powder-averaged and single-crystallite Cα lineshapes. In this set of simulations, we ignored all interactions between Cα and Cβ, as well as the J-coupling interaction between C′ and Cα. The results for the spinning frequency of 9 kHz are plotted in Fig. 9a. The powder averaged Cα lineshape is doublet-like, with the downfield doublet component having lower intensity. Single crystallite spectra with $\alpha = 0$ and β values of 95° and 135° correspond to the near-extreme values of the dipolar shift.

Fig. 9b shows a comparison between the numerical simulations (crosses) and the analytical dependence of the dipolar shift on angle β (solid line) given by Eq. (26). Even though Eq. (26) was derived assuming vanishing chemical shift anisotropy, the agreement is very good for both, Cα and C′ (data not shown). The function given in Eq. (26) is periodic, with the minimum dipolar shift of −42 Hz occurring at $\beta = 43.4°$ and 136.6°, and the maximum shift of 11 Hz occurring at $\beta = 90°$. We conclude, that in the intermediate spinning regime at moderate applied magnetic field strengths, the extent of inhomogeneous linebroadening due to the second-order dipolar shift is comparable to the magnitude of

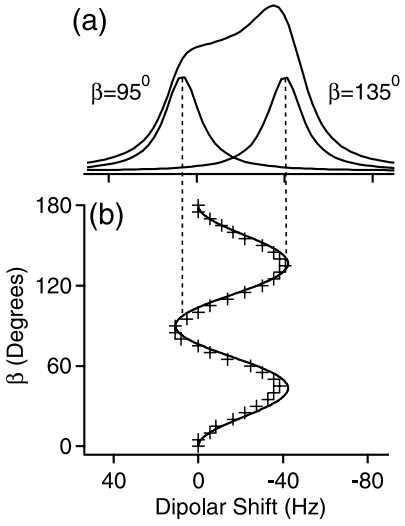

Fig. 9. Orientation dependence of the second-order dipolar shift. (a) Simulated $^{13}C\alpha$ resonance with all J-coupling interactions and dipolar coupling to Cβ turned off. The graph also shows the spectra of individual crystallites with $\beta = 95°$ and 135°, corresponding to the near-extreme values of the second-order dipolar shift. (b) Dependence of the second-order dipolar shift on angle β obtained from Eq. (26) (—) and numerical simulations (+).

J-coupling interactions. In the absence of chemical shift anisotropy, the powder-averaged C′ lineshape is an exact mirror image of the Cα lineshape, with the downfield "doublet" component having a higher intensity.

It is evident from Figs. 7 and 8 that the J-decoupled and free precession spectra do not match the simulations exactly. In fact, it appears that the decoupled C′ and Cα lineshapes are inverted relative to the simulated lineshapes. To explain this phenomenon, we invoked the orientation dependence of transfer efficiency of the mixing sequence that we used in the 2D experiments, ZQ ^{13}C–^{15}N double cross-polarization. As a first step, we constructed powder-averaged spectra corresponding to the different regions of the curve described by Eq. (26). The spectra, $S(\Delta^{(2)})$, were constructed according to the following equation:

$$S(\Delta^{(2)}(\beta)) = \frac{\sin\beta}{\left|\mathrm{d}\Delta^{(2)}/\mathrm{d}\beta\right|} \tag{27}$$

and are presented in Fig. 10a, where the blue trace corresponds to the β angle in the ranges of 0–43.4° and 136.6–180°, and the red trace corresponds to the β angle in the range of 43.4–136.6°. The dotted line shows the sum of the two powder patterns. The asymmetry of the dipolar pattern is similar to that obtained in numerical simulations, with the downfield component having a higher intensity.

For the on-resonance transfer in a double cross-polarization experiment, the effective ZQ dipolar-coupling element, d_1, is given by the following equation [33]:

$$d_1 = -b_{CN}\frac{\sin 2\beta'}{\sqrt{8}}, \tag{28}$$

where β' is the angle between the C–N inter-nuclear vector and the rotor axis. For the C′–N nuclear pair in alanine, there exists an approximate geometric relationship between β and β':

$$\beta' \cong \beta + 34°. \tag{29}$$

To relate the lineshape to the transfer efficiency, in Fig. 10b, we show a parametric plot of d_1 versus the second dipolar shift, $\Delta^{(2)}$. The starting point in the curve corresponds to $\beta = 0°$ and is marked as such in the graph. Parts of the curve are color-coded according to the same scheme as in Fig. 10a. It is clear from the comparison of parts a and b of Fig. 10, that the crystallites with higher statistical weight have a smaller effective dipolar-coupling element. When the mixing sequence in the indirect dimension is implemented, the resulting lineshape, while being inhomogeneously broadened by the second-order dipolar shift, reflects the orientation dependence of the transfer efficiency in its intensity distribution. Note that the apparent inversion of the Cα dipolar pattern cannot be satisfactorily explained by invoking the same arguments as for C′. The situation with Cα is more complex due to the presence of strong interactions with ^1H that need to be taken into account.

To summarize, C′ and Cα spins will experience inhomogeneous line broadening due to the presence of second-order dipolar shift. For alanine, this broadening is 53 Hz, which is comparable to the J-coupling constant between the two carbons. The intensity distribution found in C′ and Cα lineshapes is determined by the orientation dependences of the second-order dipolar shift and mixing sequence.

3. Conclusions and practical considerations

We have characterized the performance of the J-decoupling sequence for two spinning frequencies, 5 and 9 kHz, focusing on the C′ and Cα atoms of alanine. In accordance with the findings of Straus et al. [8], the J-coupling interactions can be entirely removed in the evolution period of 2D experiments. At a spinning frequency of 9 kHz, which falls between $n = 1$ and $n = 2$ rotational resonance conditions for the C′–Cα pair, the J-decoupled resonances are inhomogeneously broadened by the orientation-dependent second-order dipolar shift. At 5 kHz, linebroadening due to the second-order shift is negligible, giving an experimental decoupled linewidth of 36 Hz for the C′ carbon.

While one can achieve better spectral resolution at low spinning frequencies, signal loss due to the CSA can be very substantial. In addition, some mixing sequences

could be problematic to implement. Therefore, the spinning frequency of 90 ppm appears to be the most practical for protein spectroscopy. We have shown that, at this spinning frequency, the contribution of the second-order dipolar shift to the linewidth is comparable to that of the homo-nuclear *J*-coupling interactions and can reach 53 Hz for alanine. We expect to observe the same behavior in proteins due to the similarity of the tensorial interactions [34]. Fig. 11 shows the ^{13}CO cross-sections of the free-precession (FP) and *J*-decoupled (DEC) 2D ^{15}N–^{13}CO double cross-polarization spectra of uniformly ^{13}C,^{15}N-enriched human ubiquitin. The cross-sections were taken through the ^{15}N resonance at 112.2 ppm, and correspond to three amino acid residues. At a spinning frequency of 9 kHz, we observe the same characteristic triplet-like lineshape as for the alanine C′ in the free precession spectra. In the *J*-decoupled protein spectrum, the doublet-like features originating from the second-order dipolar shift are resolved for the two resonances. The performance of *J*-decoupling in uniformly ^{13}C,^{15}N-enriched protein samples will be the subject of a future publication.

One practical question that arises from the conclusions of this paper is whether the second-order dipolar shift can be removed spectroscopically in uniformly ^{13}C,^{15}N-enriched protein samples. The second-order effects transform as a fourth-rank tensor [35,36]. Consequently, no current MAS method can be used to remove the linebroadening. SIMPSON simulations of the Lee–Goldburg pulse sequence [37–39] applied to the ^{13}C spins in alanine, showed that this pulse sequence fails to remove the effect of the "flip-flop" part of the dipolar Hamiltonian and leaves the lineshape unchanged.

In addition to the inhomogeneous linebroadening, a direct consequence of Eq. (26) is the spinning frequency-dependent shift in the resonance position of the two dipolar-coupled nuclei. This shift, which can be easily obtained by averaging Eq. (26) over angle β, should be taken into account when comparing nD ssNMR protein spectra recorded at different spinning frequencies.

Another point of practical interest is the comparison of the contributions of the homo-nuclear dipolar coupling interactions to the ^{13}C linewidth at moderate and high applied magnetic field strengths. Fig. 12 shows the simulated C′ resonances at 800 MHz (a,c) and 400 MHz (b,d). Graphs a and b correspond to the spinning frequency of 35 kHz. The broad $n = 1$ rotational resonance condition at 800 MHz results in broader doublet com-

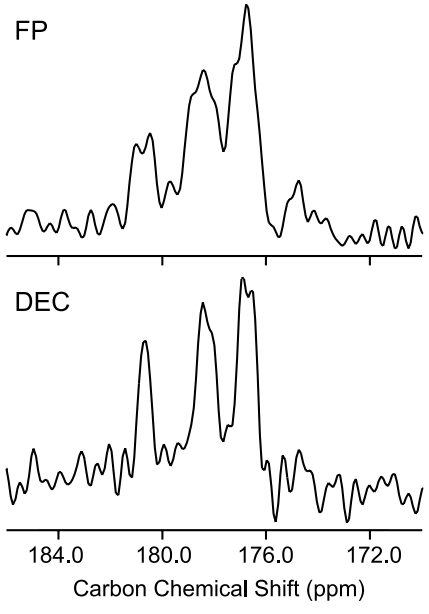

Fig. 11. ^{13}CO cross-sections of the free-precession (FP) and *J*-decoupled (DEC) 2D ^{15}N–^{13}CO double cross-polarization spectra of uniformly ^{13}C,^{15}N-enriched human ubiquitin. The cross-sections were taken through the ^{15}N resonance at 112.2 ppm. The ZQ ^{13}C–^{15}N double cross-polarization experiments with and without *J*-decoupling were carried out at a spinning frequency of 9 kHz, using approximately the same parameters as described in Fig. 7 caption.

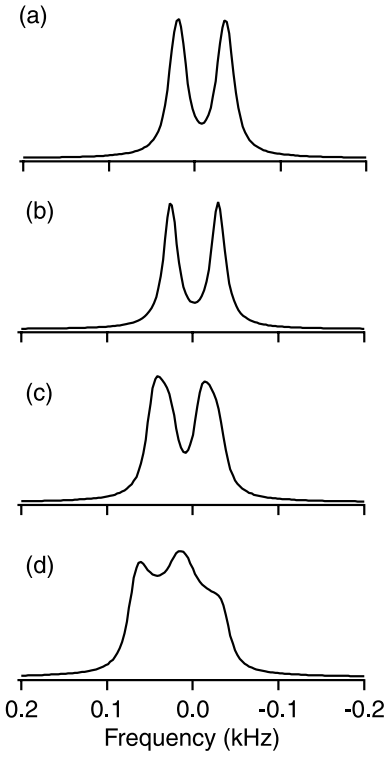

Fig. 12. Simulated ^{13}C′ lineshapes at (a) field strength of 800 MHz, spinning frequency of 35 kHz; (b) field strength of 400 MHz, spinning frequency of 35 kHz; (c) field strength of 800 MHz, spinning frequency of 18 kHz; (d) field strength of 400 MHz, spinning frequency of 9 kHz. At a spinning frequency of 35 kHz (a,b), the linewidths of the C′ doublet components are smaller at 400 MHz than at 800 MHz, due to the broad $n = 1$ C′–Cα rotational resonance condition at 800 MHz. At a spinning frequency of 90 ppm (c,d), the homo-nuclear dipolar coupling is truncated by the chemical shift difference at 800 MHz compared to 400 MHz.

ponents compared to those of 400 MHz. Graphs c and d show the C′ lineshapes at a spinning frequency of 90 ppm, which corresponds to 9 kHz at 400 MHz and 18 kHz at 800 MHz. The contribution of the dipolar coupling to the linewidth at 800 MHz is noticeable despite its obvious truncation by the chemical shift difference. Since the major contribution to the ^{13}C linewidth at high applied magnetic field strengths comes from the *J*-coupling interactions, *J*-decoupling could lead to a substantial improvement of the spectral quality for proteins that are expected to have congested nD ssNMR spectra. Since membrane proteins typically have little variety in their amino acid composition and secondary structure, their spectra could benefit from *J*-decoupling, provided the linewidths are not dominated by the conformational heterogeneity of the sample.

4. Experimental

Uniformly ^{13}C,^{15}N-enriched alanine was purchased from Cambridge Isotopes (Andover, MA). The alanine sample was doped with 0.01% (molar) $CuCl_2$ and crystallized by slow solvent evaporation from a saturated water solution.

All solid-state NMR experiments were carried out on a 400 MHz Infinity Plus NMR spectrometer equipped with a 4 mm T3 MAS probe (Varian/Chemagnetics). 1D ^{13}C CP MAS spectra of alanine were recorded using a ramped ^{1}H–^{13}C cross-polarization sequence [40] with 90 kHz TPPM [41] ^{1}H decoupling during acquisition. The spinning frequency was varied from 2 to 15 kHz in steps of 1 kHz and controlled with an accuracy of ± 3 Hz.

For the measurements of DANTE inversion profiles, we combined a cross-polarization preparation sequence with a pulse width-modulated DANTE pulse train. In this work, we have implemented a Gaussian modulation function with 5% truncation amplitude. However, other pulse-shaping functions can be used as well [22]. To minimize the effect of pulse transients, a pair of pulses with a 180° phase shift was substituted for each pulse in the DANTE sequence [42]. The carrier frequency was incremented in steps of 40 Hz. The selective pulse and the receiver were phase-cycled according to the spin pinging sequence [19], which ensured subtraction of signals originating from the out-of-band spins. The total length of the DANTE sequence was adjusted to be a multiple of the rotor periods, while no rotor-synchronization of the actual pulse train was employed. An identical pulse sequence was used for the calibration of DANTE pulses.

2D selective double cross-polarization (DCP) experiments [33] were performed in order to record the carboxyl (C′) and Cα 2D spectra of alanine. Fig. 1 shows a cartoon of the pulse sequence that incorporates ω_1-decoupling. Typically, the DANTE pulse train consisted of 21–41 pulses and its duration, $m * T_r$ (see Fig. 1), was set according to the bandwidth requirement for a given spin type. The choice of m is discussed in more detail in Section 2.1.1. Rotor-synchronization of sampling and the decoupling element was essential for obtaining artifact-free spectra. The TPPM ^{1}H decoupling field strength of 93 kHz and CW field strength of 100 kHz was used during evolution and mixing, respectively. ^{13}C–^{15}N ZQ transfers were carried out with the following field strength parameters: ^{15}N 12.5 kHz and ^{13}C 17.5 kHz at 5 kHz spinning frequency, and ^{15}N 13.5 kHz and ^{13}C 22.5 kHz at 9 kHz spinning frequency.

The ^{13}C–^{13}C *J*-coupling constants in uniformly ^{13}C,^{15}N-enriched alanine were measured in a solution NMR experiment, performed on a Bruker DRX-300 spectrometer. Coupling constants obtained from this analysis are presented in Table 1.

Simulations of lineshapes, magnetization trajectories, and inversion profiles for alanine (three-spin system) were carried out using SIMPSON simulation program [24]. Euler angles of the chemical shift anisotropy (CSA) tensor of the carbon atoms of alanine were derived from the direction cosines given by Naito et al. [43]. In that work, the CSA tensor of the Cβ carbon was given as a left-handed tensor as noted previously by several authors [44–46]. The tensor was forced to conform to the right-handed notation by inverting the sign of the principal Y axis. The inter-atomic distances and direction cosines of the dipolar coupling tensors were calculated from the crystal structure of alanine [47]. The details on extracting tensor parameters from direction cosines are described elsewhere [48]. The CSA and dipolar coupling parameters used in SIMPSON simulations are presented in Table 1. Typically, 376 α/β orientations distributed according to the ZCW algorithm and 20 γ angles were used in the simulations.

Acknowledgments

This work was supported by the NSF Grant MCB 83581. The authors thank Dr. Lyndon Emsley for making Ref. [31] available prior to publication.

References

[1] A. McDermott, T. Polenova, A. Bockmann, K.W. Zilm, E.K. Paulsen, R.W. Martin, G.T. Montelione, Partial NMR assignments for uniformly (C-13, N-15)-enriched BPTI in the solid state, J. Biomol. NMR 16 (2000) 209–219.

[2] T.I. Igumenova, R. Martin, C.M. Rienstra, E. Paulson, A.J. Wand, K.W. Zilm, A.E. McDermott, Sample preparation and solid-state NMR spectroscopy of uniformly (C-13, N-15)-labeled human ubiquitin, Poster No. 107, Experimental NMR Conference, Orlando, 2001.

[3] J. Cavanagh, W. Fairbrother, A.G. Palmer, N.J. Skelton, Protein NMR Spectroscopy: Principles and Practice, Academic Press, New York, 1996, pp. 480–481.
[4] D.M. LeMaster, D.M. Kushlan, Dynamical mapping of *E. coli* thioredoxin via C-13 NMR relaxation analysis, J. Am. Chem. Soc. 118 (1996) 9255–9264.
[5] M. Hong, Determination of multiple phi-torsion angles in proteins by selective and extensive C-13 labeling and two-dimensional solid-state NMR, J. Magn. Reson. 139 (1999) 389–401.
[6] M. Hong, K. Jakes, Selective and extensive C-13 labeling of a membrane protein for solid-state NMR investigations, J. Biomol. NMR 14 (1999) 71–74.
[7] R. Bruschweiler, C. Griesinger, O.W. Sorensen, R.R. Ernst, Combined use of hard and soft pulses for ω1 decoupling in two-dimensional NMR-spectroscopy, J. Magn. Reson. 78 (1988) 178–185.
[8] S.K. Straus, T. Bremi, R.R. Ernst, Resolution enhancement by homo-nuclear J decoupling in solid-state MAS NMR, Chem. Phys. Lett. 262 (1996) 709–715.
[9] S. Grzesiek, A. Bax, Improved 3D triple-resonance NMR techniques applied to a 31-kDa protein, J. Magn. Reson. 96 (1992) 432–440.
[10] G.W. Vuister, A. Bax, Measurement of 2-bond and 3-bond proton to methyl-carbon *J*-couplings in proteins uniformly enriched with C-13, J. Magn. Reson. B 102 (1993) 228–231.
[11] T. Yamazaki, W. Lee, C.H. Arrowsmith, D.R. Muhandiram, L.E. Kay, A suite of triple-resonance NMR experiments for the backbone assignment of N-15, C-13, H-2 labeled proteins with high-sensitivity, J. Am. Chem. Soc. 116 (1994) 11655–11666.
[12] M.A. McCoy, L. Mueller, Coherence quenching induced by frequency-selective homo-nuclear decoupling, J. Magn. Reson. 98 (1992) 674–679.
[13] M.A. McCoy, L. Mueller, Selective shaped pulse decoupling in NMR—homo-nuclear [C-13]carbonyl decoupling, J. Am. Chem. Soc. 114 (1992) 2108–2112.
[14] E. Kupce, G. Wagner, Multisite band-selective decoupling in proteins, J. Magn. Reson. B 110 (1996) 309–312.
[15] H. Matsuo, E. Kupce, H.J. Li, G. Wagner, Increased sensitivity in HNCA and HN(CO)CA experiments by selective Cβ decoupling, J. Magn. Reson. B 113 (1996) 91–96.
[16] S.K. Straus, T. Bremi, R.R. Ernst, Experiments and strategies for the assignment of fully C-13/N-15-labelled polypeptides by solid state NMR, J. Biomol. NMR 12 (1998) 39–50.
[17] J. Cavanagh, pp. 136–137.
[18] G. Bodenhausen, R. Freeman, G.A. Morris, Simple pulse sequence for selective excitation in Fourier-transform NMR, J. Magn. Reson. 23 (1976) 171–175.
[19] X.L. Wu, P. Xu, R. Freeman, A new kind of selective excitation sequence, J. Magn. Reson. 83 (1989) 404–410.
[20] J. Friedrich, S. Davies, R. Freeman, Shaped selective pulses for coherence-transfer experiments, J. Magn. Reson. 75 (1987) 390–395.
[21] H. Geen, S. Wimperis, R. Freeman, Band-selective pulses without phase distortion—a simulated annealing approach, J. Magn. Reson. 85 (1989) 620–627.
[22] C. Roumestand, J. Mispelter, C. Austruy, D. Canet, The use of band filtering in multidimensional NMR—evaluation of 2 user-friendly techniques, J. Magn. Reson. B 109 (1995) 153–163.
[23] M.H. Levitt, D.P. Raleigh, F. Creuzet, R.G. Griffin, Theory and simulations of homo-nuclear spin pair systems in rotating solids, J. Chem. Phys. 92 (1990) 6347–6364.
[24] M. Bak, J.T. Rasmussen, N.C. Nielsen, SIMPSON: a general simulation program for solid-state NMR spectroscopy, J. Magn. Reson. 147 (2000) 296–330.
[25] P. Caravatti, G. Bodenhausen, R.R. Ernst, Selective pulse experiments in high-resolution solid-state NMR, J. Magn. Reson. 55 (1983) 88–103.
[26] G.A. Morris, R. Freeman, Selective excitation in Fourier-transform nuclear magnetic-resonance, J. Magn. Reson. 29 (1978) 433–462.
[27] M.H. Levitt, Why do spinning sidebands have the same phase, J. Magn. Reson. 82 (1989) 427–433.
[28] N.C. Nielsen, H. Bildsoe, H.J. Jakobsen, M.H. Levitt, Double-quantum homo-nuclear rotary resonance—efficient dipolar recovery in magic-angle-spinning nuclear-magnetic-resonance, J. Chem. Phys. 101 (1994) 1805–1812.
[29] D.P. Raleigh, G.S. Harbison, T.G. Neiss, J.E. Roberts, R.G. Griffin, Homo-nuclear *J*-couplings and rotationally induced side-band enhancements in NMR-spectra of rotating solids, Chem. Phys. Lett. 138 (1987) 285–290.
[30] Z.H. Gan, D.M. Grant, Pseudo-spin rotational resonance and homo-nuclear dipolar NMR of rotating solids, Mol. Phys. 67 (1989) 1419–1430.
[31] L. Duma, S. Hediger, A. Lesage, D. Sakellariou, L. Emsley, Carbon-13 lineshapes in solid-state NMR of labeled compounds. Effects of coherent CSA-dipolar cross correlation, J. Magn. Reson. 162 (2003) 90–101.
[32] B.H. Meier, W.L. Earl, A double-quantum filter for rotating solids, J. Am. Chem. Soc. 109 (1987) 7937–7942.
[33] M. Baldus, A.T. Petkova, J. Herzfeld, R.G. Griffin, Cross polarization in the tilted frame: Assignment and spectral simplification in heteronuclear spin systems, Mol. Phys. 95 (1998) 1197–1207.
[34] H.H. Sun, L.K. Sanders, E. Oldfield, Carbon-13 NMR shielding in the twenty common amino acids: comparisons with experimental results in proteins, J. Am. Chem. Soc. 124 (2002) 5486–5495.
[35] M. Ernst, S. Bush, A.C. Kolbert, A. Pines, Second-order recoupling of chemical-shielding and dipolar-coupling tensors under spin decoupling in solid-state NMR, J. Chem. Phys. 105 (1996) 3387–3397.
[36] M. Ernst, A.C. Kolbert, K. Schmidt-Rohr, A. Pines, Isotropic second-order dipolar shifts in the rotating frame, J. Chem. Phys. 104 (1996) 8258–8268.
[37] A. Bielecki, A.C. Kolbert, H.J.M. de Groot, R.G. Griffin, M.H. Levitt, Frequency-switched Lee–Goldburg sequences in solids, Adv. Magn. Reson. 14 (1990) 111–124.
[38] E. Vinogradov, P.K. Madhu, S. Vega, Proton spectroscopy in solid state nuclear magnetic resonance with windowed phase modulated Lee–Goldburg decoupling sequences, Chem. Phys. Lett. 354 (2002) 193–202.
[39] E. Vinogradov, P.K. Madhu, S. Vega, High-resolution proton solid-state NMR spectroscopy by phase-modulated Lee–Goldburg experiment, Chem. Phys. Lett. 314 (1999) 443–450.
[40] G. Metz, X.L. Wu, S.O. Smith, Ramped-amplitude cross-polarization in magic-angle-spinning NMR, J. Magn. Reson. A 110 (1994) 219–227.
[41] A.E. Bennett, C.M. Rienstra, M. Auger, K.V. Lakshmi, R.G. Griffin, Heteronuclear decoupling in rotating solids, J. Chem. Phys. 103 (1995) 6951–6958.
[42] T. Nakai, C.A. McDowell, The necessity for synchronization in DANTE experiments with rotating samples—reclamation of the asynchronous DANTE pulse train by combination with the TOSS sequence, J. Magn. Reson. 90 (1990) 426–432.
[43] A. Naito, S. Ganapathy, K. Akasaka, C.A. McDowell, Chemical shielding tensor and C-13–N-14 dipolar splitting in single crystals of L-alanine, J. Chem. Phys. 74 (1981) 3190–3197.
[44] W.L. Zhu, C.A. Klug, J. Schaefer, Measurement of dipolar coupling within isolated spin-1/2 homo-nuclear pairs by CEDRA NMR, J. Magn. Reson. A 108 (1994) 121–123.

[45] M. Bak, N.C. Nielsen, Relative orientation of chemical shielding and dipolar coupling tensors: mixed single- and double-quantum homo-nuclear rotary resonance nuclear magnetic resonance of rotating solids, J. Chem. Phys. 106 (1997) 7587–7599.
[46] M.H. Levitt, M. Eden, Numerical simulation of periodic nuclear magnetic resonance problems: fast calculation of carousel averages, Mol. Phys. 95 (1998) 879–890.
[47] M.S. Lehmann, T.F. Koetzle, W.C. Hamilton, Precision neutron-diffraction structure determination of protein and nucleic acid components. 1. Crystal and molecular structure of amino-acid L-alanine, J. Am. Chem. Soc. 94 (1972) 2657–2660.
[48] T.I. Igumenova, Ph.D. thesis, Columbia University, New York, 2003.